Engineering with Computers (2022) 38:1679–1696
https://doi.org/10.1007/s00366-020-01130-8

ORIGINAL ARTICLE

A computational framework for propagated waves in a sandwich doubly curved nanocomposite panel

M. S. H. Al-Furjan[1,2] · Mostafa Habibi[3,4] · Dong won Jung[5] · Seyedehfatemeh Sadeghi[6] · Hamed Safarpour[7] · Abdelouahed Tounsi[8] · Guojin Chen[1]

Received: 1 June 2020 / Accepted: 24 July 2020 / Published online: 3 August 2020

Abstract
In the current report, characteristics of the propagated wave in a sandwich structure with a soft core and multi-hybrid nanocomposite (MHC) face sheets are investigated. The higher-order shear deformable theory (HSDT) is applied to formulate the stresses and strains. Rule of the mixture and modified Halpin–Tsai model are engaged to provide the effective material constant of the multi-hybrid nanocomposite face sheets of the sandwich panel. By employing Hamilton's principle, the governing equations of the structure are derived. Via the compatibility rule, the bonding between the composite layers and a soft core is modeled. Afterward, a parametric study is carried out to investigate the effects of the CNTs' weight fraction, core to total thickness ratio, various FG face sheet patterns, small radius to total thickness ratio, and carbon fiber angel on the phase velocity of the FML panel. The results show that the sensitivity of the phase velocity of the FML panel to the W_{CNT} and different FG face sheet patterns can decrease when we consider the core of the panel more much thicker. It is also observed that the effects of fiber angel and core to total thickness ratio on the phase velocity of the FML panel are hardly dependent on the wavenumber. The presented study outputs can be used in ultrasonic inspection techniques and structural health monitoring.

Keywords Multi-scale hybrid nanocomposite reinforcement · Elastic core · Doubly curved panel · Compatibility equations · Phase velocity

✉ Mostafa Habibi
mostafahabibi@duytan.edu.vn

✉ Dong won Jung
jdwcheju@jejunu.ac.kr

✉ Abdelouahed Tounsi
tou_abdel@yahoo.com

M. S. H. Al-Furjan
Rayan@hdu.edu.cn

Seyedehfatemeh Sadeghi
drsadeghi.fatemeh@gmail.com

Hamed Safarpour
Hamed_safarpor@yahoo.com

Guojin Chen
Chenguojin@163.com

1 School of Mechanical Engineering, Hangzhou Dianzi University, Hangzhou 310018, China

2 School of Materials Science and Engineering, State Key Laboratory of Silicon Materials, Zhejiang University, Hangzhou 310027, China

3 Institute of Research and Development, Duy Tan University, Da Nang 550000, Vietnam

4 Faculty of Electrical–Electronic Engineering, Duy Tan University, Da Nang 550000, Vietnam

5 School of Mechanical Engineering, Jeju National University, Jeju 690-756, Jeju-do, Korea

6 Department of Prosthetic, School of Dentistry, Shahid Beheshti University of Medical Sciences, Tehran, Iran

7 Faculty of Engineering, Department of Mechanics, Imam Khomeini International University, Qazvin, Iran

8 Civil Engineering Department, Material and Hydrology Laboratory, Faculty of Technology, University of Sidi Bel Abbes, Sidi Bel Abbes, Algeria

1 Introduction

Up to now, huge research is proved that the compositionally structures have a marvelous thermo-electro-mechanical property [1–3] and this issue is being an important reason to take the attention of all engineering fields for having efficient productions with the aid of composite structure, especially carbon-based nanofillers reinforced structure [4–10]. In addition to what is mentioned owing to the wide applications of wave propagation analysis in structural health monitoring, most recently, an interesting field of research has been started in scholar which is called wave propagation response [11–13]. In addition, the properties of reinforcements make them an appropriate choice to be used in chemistry, physics, electrical engineering [14–26], materials science [10], and engineering applications [27–35].

By considering the mentioned necessities and in the field of wave propagation in composite beams and plates, Ebrahime et al. [36] could present a paper to investigate the wave propagation of the sandwich plate in which the structure is embedded in a nonlinear foundation. Also, they considered a magnetic environment in their model and used the classical theory for doing their computational formulation. Based on their result, as the magnetic layer will play the most important role on the wave response of the sandwich plate [37]. presented a comprehensive formulation on the wave dispersion of a high speed rotating 2D-FG nanobeam. They used nonlocal theory for consideration of the couple stress in the nanomechanics effect on the wave response of the structure. They could solve their complex formulation via an analytical method and they reported that the rotating speed is the most effective parameter. By employing the new version couple stress theory, Global matrix, and Legendre orthogonal polynomial methods, and, Liu et al. [38] had a try for reporting the characteristics of the propagated wave in a micro FG plate. They reported that by controlling the couple stress, we will have the grater phase velocity in the aspect of wave propagation. Ebrahimi et al. [39] succeeded in publishing a paper in which a computational framework is developed for investigation wave behavior in a thermally affected nonlocal beam which is made by FG materials. One of their assumptions was that the nanobeam is under high-speed rotation and is located in a thermal environment. They presented a lot of results but the most significant one was that changing the rotating speed can provide some novel results on the wave propagation in the nanostructure. In a novel work, Barati [40] showed the behavior of propagated wave in the porous nanobeam with attention to the nonlocality via strain–stress gradient theory. Gao et al. [41] could report a mathematical framework to analyze the propagated wave in a GPLs reinforced porous FG plate via a well-known mixture method. Based on their result, porosity and GPLs weight fraction are two important parameters in the field of structural health monitoring via wave propagation method. Ebrahimi et al. [42] were able to provide results on the characteristics propagated waves in a compositionally nonlocal plate in which the structure located in a high-temperature environment. Also, they consider the shear deformation in each element of the structure. They found that without doubt the nonlocal effect has a bolded role on the characteristics of propagated waves. Safaei et al. [43] tried to report characteristics of the propagated waves in a CNTs reinforced FG thermoelastic plate via the high order ready plat theory and Mori–Tanaka method. Their important achievement was that the thermal stress and adding small amount of CNTs can make a remarkable effect on the wave velocity in the structure. The static and dynamic stabilities of the reinforced nanocomposite structures are presented in some researches [44–50] by having attention to the impacts of honeycomb core, porosity distributions, and transverse dynamic loads via higher-order theories. Many researchers [51–56] studied the behavior and stability of the FG multilayer composite and isotropic materials.

In the field of characteristics propagated waves in the shell, Bakhtiari et al. [57] provided some results on the wave propagation of the FG shell in which fluid flow through the shell is considered. Ebrahimi et al. [58] studied the wave response in a high-speed rotating nanoshell with a GPLs reinforced compositionally core and patched piezoelectric face sheet. They claimed that if the rotating should be controlled for improving the phase velocity of the nanoshell. The dispersion behavior of the wave in the MHC reinforced shell is investigated by Ebrahimi et al. [59]. They used the lowest order shear deformation theory and eigenvalue problem for providing their formulation and results. They found out that the impact of nanosize reinforcements is more effective than the macro size reinforcements for improving the phase velocity of the compositionally shell. Karami et al. [60] developed a mathematical model for literature in which wave dispersion in an imperfect nanoshell via NSG and HSD theories is analyzed. They provided some evidences that sensitivity of the prospected waves to the nonlocal effects, temperature, and humidity in the porous material should be considered. The vibration and buckling/post-buckling responses of the curved structures are investigated in some researches [61–67]. A key issue in various engineering field is that the prediction of the properties, behavior, and performance of different systems is an important aspect [68–77]. Also, some researchers tried to predict the static and dynamic properties of different structures and materials via neural network solution [78–84]. In addtion, many studies reported the application of applied soft computing method for prediction of the behavior of complex system [85–92].

In the field of analysis, the wave propagation in the smart structure, Li et al. [93] succeeded in publishing an article in which they examined the wave propagation of a smart plate via a semi-analytical method. They modeled a GPLs reinforced plate which is covered with a piezoelectric actuator. They used the Reissner–Mindlin plate theory and Hamilton's principle for developing their computational approach and did the formulation. The application of their result is that GPLs in a matrix can play a positive role in structural health monitoring and improve wave propagation in the structures, especially smart structures. Ebrahimi et al. [94] developed a mathematical model for literature in which wave dispersion of a smart sandwich nanoplate by considering the nanosize effect via nonlocal strain gradient theory and the sandwich structure is made of ceramic face sheets and magnetostrictive core. Abad et al. [95] published an article in which they presented a formulation about the wave propagation problem of a somewhat sandwich thick plate. They smarted the plate by patching a piezoelectric layer on the top face of the structure and they considered Maxwell's assumptions in their computational approach. Habibi et al. [96] studied the wave response in a nanoshell with a GPLs reinforced compositionally core and patched piezoelectric face sheet. When they compared their result with molecular simulation, it can be seen that the nonlocality should be considered via NSGT. As a practical outcome they reported that the thickness of the smart layer will have more effect on the characteristics propagated waves in the nanoshell.

Based on the extremely detailed exploration in the literature by the authors, no one can claim that there is a study on the wave propagation of the doubly curved panel.

Therefore, characteristics of the propagated wave in a sandwich structure with a soft core and multi-hybrid nanocomposite face sheets are investigated. The HSDT is applied to formulate the stresses and strains. Rule of the mixture and modified Halpin–Tsai model are engaged to provide the effective material constant of the multi-hybrid nanocomposite face sheets of the sandwich panel. By employing Hamilton's principle, the governing equations of the structure are derived. Via the compatibility rule, the bonding between the smart layer and the soft core is modeled. The results show that, CNT's weight fraction, core to total thickness ratio, various FG face sheet patterns, small radius to total thickness ratio, and carbon fiber angel have an important role in the phase velocity of the FML panel.

2 Mathematical modeling

Figure 1 shows a sandwich doubly curved panel. The effective thickness ($h_b+h_c+h_t$) and the middle surface radius of the doubly curved panel are presented by h_{eff} and R, respectively. Besides, h_b h_c, and h_p are the thickness of the multi-hybrid nanocomposite reinforcement at the top layer, the core layer, and the multi-hybrid nanocomposite reinforcement at the bottom layer, respectively.

2.1 MHC reinforcement

The procedure of homogenization is made of two main steps based upon the Halpin–Tsai model together with a micromechanical theory. The first stage is engaged with computing the effective characteristics of the composite reinforced with CF as following [97]:

$$E_{11} = V_{\mathrm{F}} E_{11}^{\mathrm{F}} + V_{\mathrm{NCM}} E^{\mathrm{NCM}}, \tag{1}$$

$$\frac{1}{E_{22}} = 1/E_{22}^{\mathrm{F}} + V_{\mathrm{NCM}}/E^{\mathrm{NCM}} - V_{\mathrm{F}} V_{\mathrm{NCM}} \\ -\frac{(\nu^{\mathrm{F}})^2 E^{\mathrm{NCM}}/E_{22}^{\mathrm{F}} + (\nu^{\mathrm{NCM}})^2 E_{22}^{\mathrm{F}}/E^{M} - 2\nu^{\mathrm{NCM}}\nu^{\mathrm{F}}}{V_{\mathrm{F}} E_{22}^{\mathrm{F}} + V_{\mathrm{NCM}} E^{\mathrm{NCM}}}, \tag{2}$$

$$\frac{1}{G_{12}} = \frac{V_{\mathrm{NCM}}}{G^{\mathrm{NCM}}} + \frac{V_{\mathrm{F}}}{G_{12}^{\mathrm{F}}}, \tag{3}$$

$$\rho = V_{\mathrm{F}} \rho^{\mathrm{F}} + V_{\mathrm{NCM}} \rho^{\mathrm{NCM}}, \tag{4}$$

$$\nu_{12} = V_{\mathrm{F}} \nu^{\mathrm{F}} + V_{\mathrm{NCM}} \nu^{\mathrm{NCM}}. \tag{5}$$

Here, elasticity modulus, mass density, Poisson's ratio, and shear modulus are symbolled via $\rho,\ E,\ G$ and ν. The superscripts of the matrix and fiber are NCM and F, respectively. Add the carbon fiber volume fraction (V_{F}) to the nanocomposite matrix volume fraction (V_{NCM}) is one.

$$V_{\mathrm{F}} + V_{\mathrm{NCM}} = 1. \tag{6}$$

The second step is organized to obtain the effective characteristics of the nanocomposite matrix reinforced with CNTs with the aid of the extended Halpin–Tsai micromechanics as follows [97]:

$$E^{j} = \frac{5}{8}\left(\frac{1 + 2\beta_{dd} V_{\mathrm{CNT}}}{1 - \beta_{dd} V_{\mathrm{CNT}}}\right) E^{M} + \frac{3}{8}\left(\frac{\beta_{dl} V_{\mathrm{CNT}} (2 l^{CNT}/d^{CNT}) + 1}{1 - \beta_{dl} V_{\mathrm{CNT}}}\right). \tag{7}$$

Here, β_{dd} and β_{dl} would be computed as the following expression:

$$\beta_{dl} = (E_{11}^{CNT}/E^{M}) - (d^{CNT}/4t^{CNT})/(E_{11}^{CNT}/E^{M}) + (l^{CNT}/2t^{CNT}), \\ \beta_{dd} = (E_{11}^{CNT}/E^{M}) - (d^{CNT}/4t^{CNT})/(E_{11}^{CNT}/E^{M}) + (d^{CNT}/2t^{CNT}), \tag{8}$$

volume fraction, thickness, length, elasticity modulus, weight fraction, and diameter of CNTs are V_{CNT}, t^{CNT}, l^{CNT}, E^{CNT},W_{CNT}, and d^{CNT}. Also, the volume fraction of the matrix and elasticity modulus of the matrix are V_M and E^M. So, The CNTs volume fraction can be formulated as below:

$$V^*_{\mathrm{CNT}} = \frac{W_{\mathrm{CNT}}}{W_{\mathrm{CNT}} + \left(\frac{\rho^{CNT}}{\rho^{M}}\right)(1 - W_{\mathrm{CNT}})}. \quad (9)$$

Also, the effective volume fraction of CNTs can be formulated as follows:

$$\begin{aligned} V_{\mathrm{CNT}} &= V^*_{\mathrm{CNT}} \frac{\left|\xi_j\right|}{h} \text{ FG - X}, \\ V_{\mathrm{CNT}} &= V^*_{\mathrm{CNT}} \left(1 + \frac{2\xi_j}{h}\right) \text{ FG - V}, \\ V_{\mathrm{CNT}} &= V^*_{\mathrm{CNT}} \left(1 - \frac{2\xi_j}{h}\right) \text{ FG - A}. \\ V_{\mathrm{CNT}} &= V^*_{\mathrm{CNT}} \text{ FG - UD}, \end{aligned} \quad (10)$$

where $\xi_j = \left(\frac{1}{2} + \frac{1}{2N_t} - \frac{j}{N_t}\right)h$ j = 1,2,...,N_t. Furthermore, the sum of V_M and V_{CNT} as the two constituents of the nanocomposite matrix is equal to 1.

$$V_{\mathrm{CNT}} + V_M = 1. \quad (11)$$

Also, Poisson's ratio, mass density, and shear modulus will be calculated as

$$\rho^j = V_{\mathrm{CNT}}\rho^{CNT} + V_M\rho^M, \quad (12)$$

$$\nu^j = \nu^M, \quad (13)$$

$$G^j = \frac{E^j}{2\left(1 + \nu^j\right)}. \quad (14)$$

2.2 Kinematic relations

The displacement fields of the core can be given by [98]

$$\begin{aligned} u^c(x,y,z,t) &= u^c_0(x,y,t) + z_c\phi^c_x(x,y,t) - c_1 z_c^3\left[\phi^c_x(x,y,t) + \frac{\partial w^c_0(x,y,t)}{\partial x}\right], \\ v^c(x,y,z,t) &= v^c_0(x,y,t) + z_c\phi^c_y(x,y,t) - c_1 z_c^3\left[\phi^c_y(x,y,t) + \frac{\partial w^c_0(x,y,t)}{\partial y}\right], \\ w^c(x,y,z,t) &= w^c_0(x,y,t). \end{aligned} \quad (15)$$

The strain components can be given by [98, 99]

$$\begin{Bmatrix} \varepsilon^c_{xx} \\ \varepsilon^c_{yy} \\ \gamma^c_{xy} \\ \gamma^c_{xz} \\ \gamma^c_{yz} \end{Bmatrix} = \begin{bmatrix} \frac{\partial u^c_0}{\partial x} + z_c\frac{\partial \phi^c_x}{\partial x} - z_c^3 c_1\left(\frac{\partial \phi^c_x}{\partial x} + \frac{\partial^2 w^c_0}{\partial x^2}\right) + \frac{w^c_0}{R_1} \\ \frac{\partial v^c_0}{\partial y} + z_c\frac{\partial \phi^c_x}{\partial y} - z_c^3 c_1\left(\frac{\partial \phi^c_y}{\partial y} + \frac{\partial^2 w^c_0}{\partial y^2}\right) + \frac{w^c_0}{R_2} \\ \frac{\partial u^c_0}{\partial y} + \frac{\partial v^c_0}{\partial x} + z_c\left(\frac{\partial \phi^c_x}{\partial y} + \frac{\partial \phi^c_y}{\partial x}\right) - z_c^3 c_1\left(\frac{\partial \phi^c_x}{\partial y} + \frac{\partial \phi^c_y}{\partial x} + 2\frac{\partial^2 w^c_0}{\partial x \partial y}\right) \\ (1 - 3z_c^2 c_1)\left(\phi^c_x + \frac{\partial w^c_0}{\partial x}\right) \\ (1 - 3z_c^2 c_1)\left(\phi^c_y + \frac{\partial w^c_0}{\partial y}\right) \end{bmatrix}. \quad (16)$$

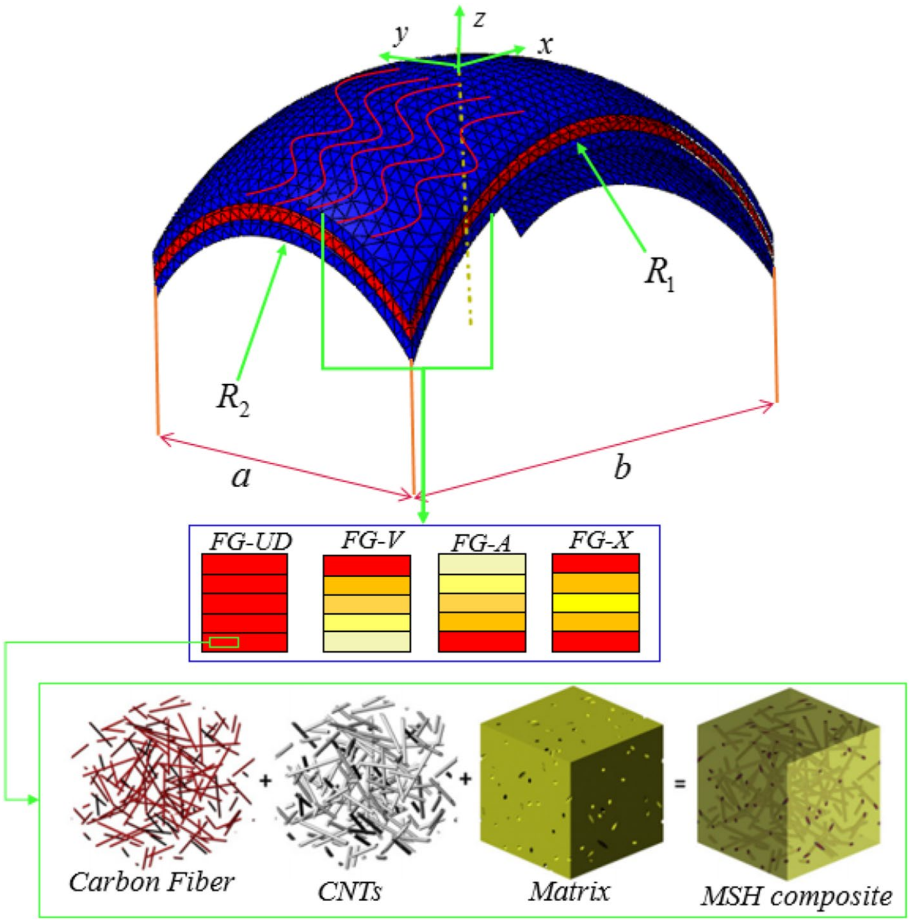

Fig. 1 A schematic of a sandwich doubly curved panel

Also, the strain–stress equations of the metal structure can be given as

$$\begin{bmatrix}\sigma^c_{xx}\\ \sigma^c_{yy}\\ \sigma^c_{xy}\\ \sigma^c_{xz}\\ \sigma^c_{yz}\end{bmatrix}=\begin{bmatrix}Q_{11} & Q_{12} & 0 & 0 & 0\\ Q_{21} & Q_{22} & 0 & 0 & 0\\ 0 & 0 & Q_{66} & 0 & 0\\ 0 & 0 & 0 & Q_{55} & 0\\ 0 & 0 & 0 & 0 & Q_{44}\end{bmatrix}\begin{bmatrix}\varepsilon^c_{xx}\\ \varepsilon^c_{yy}\\ \varepsilon^c_{xy}\\ \varepsilon^c_{xz}\\ \varepsilon^c_{yz}\end{bmatrix}. \tag{17}$$

In which [100–103]:

$$Q_{11}=Q_{22}=\frac{E_c}{1-\nu_c^2},\quad Q_{12}=Q_{21}=\frac{E_c\nu_c}{1-\nu_c^2},$$
$$Q_{44}=Q_{55}=Q_{66}=\frac{E_c}{2(1+\nu_c)}.$$

In the Eq. (17) E_c, and ν_c are Young's module and poison ratio of the metal, respectively.

2.3 Face sheets

In the present structural model for the sandwich panel, the HSDT is adopted for the face sheets. Hence, the displacement components of the top and bottom face sheets (j = t, b) are represented as

$$\begin{aligned}
u^j(x,y,z,t)&=u^j_0(x,y,t)+z_j\phi^j_x(x,y,t)-c_1z_j^3\left[\phi^j_x(x,y,t)+\frac{\partial w^j_0(x,y,t)}{\partial x}\right],\\
v^j(x,y,z,t)&=v^j_0(x,y,t)+z\phi^j_y(x,y,t)-c_1z_j^3\left[\phi^j_y(x,y,t)+\frac{\partial w^j_0(x,y,t)}{\partial y}\right],\\
w^j(x,y,z,t)&=w^j_0(x,y,t).
\end{aligned} \tag{18}$$

The strain components can be given by

$$\begin{Bmatrix} \varepsilon_{xx}^j \\ \varepsilon_{yy}^j \\ \gamma_{xy}^j \\ \gamma_{xz}^j \\ \gamma_{yz}^j \end{Bmatrix} = \begin{bmatrix} \frac{\partial u_0^j}{\partial x} + z_j \frac{\partial \phi_x^j}{\partial x} - z_j^3 c_1 \left(\frac{\partial \phi_x^j}{\partial x} + \frac{\partial^2 w_0^j}{\partial x^2} \right) + \frac{w_0^j}{R_1} \\ \frac{\partial v_0^j}{\partial y} + z_j \frac{\partial \phi_x^j}{\partial y} - z_j^3 c_1 \left(\frac{\partial \phi_y^j}{\partial y} + \frac{\partial^2 w_0^j}{\partial y^2} \right) + \frac{w_0^j}{R_2} \\ \frac{\partial u_0^j}{\partial y} + \frac{\partial v_0^j}{\partial x} + z_j \left(\frac{\partial \phi_x^j}{\partial y} + \frac{\partial \phi_y^j}{\partial x} \right) - z_j^3 c_1 \left(\frac{\partial \phi_x^j}{\partial y} + \frac{\partial \phi_y^j}{\partial x} + 2 \frac{\partial^2 w_0^j}{\partial x \partial y} \right) \\ (1 - 3 z_j^2 c_1) \left(\phi_x^j + \frac{\partial w_0^j}{\partial x} \right) \\ (1 - 3 z_j^2 c_1) \left(\phi_y^j + \frac{\partial w_0^j}{\partial y} \right) \end{bmatrix}. \tag{19}$$

Also, the strain–stress equations of the metal structure can be given as [9, 104–118]

$$\begin{bmatrix} \sigma_{xx}^j \\ \sigma_{yy}^j \\ \sigma_{xy}^j \\ \sigma_{xz}^j \\ \sigma_{yz}^j \end{bmatrix} = \begin{bmatrix} Q_{11}^j & Q_{12}^j & 0 & 0 & 0 \\ Q_{21}^j & Q_{22}^j & 0 & 0 & 0 \\ 0 & 0 & Q_{66}^j & 0 & 0 \\ 0 & 0 & 0 & Q_{55}^j & 0 \\ 0 & 0 & 0 & 0 & Q_{44}^j \end{bmatrix} \begin{bmatrix} \varepsilon_{xx}^j \\ \varepsilon_{yy}^j \\ \varepsilon_{xy}^j \\ \varepsilon_{xz}^j \\ \varepsilon_{yz}^j \end{bmatrix}, \tag{20}$$

where [119]

$$\begin{aligned} \overline{Q}_{11}^j &= Q_{11}^j \cos^4\theta + 2Q_{12}^j \sin^2\theta \cos^2\theta + Q_{22}^j \sin^4\theta, \\ \overline{Q}_{12}^j &= \left(Q_{11}^j + Q_{22} \right) \sin^2\theta \cos^2\theta + Q_{12}^j \left(\sin^4\theta + \cos^4\theta \right), \\ \overline{Q}_{22}^j &= Q_{11}^j \sin^4\theta + 2Q_{12}^j \sin^2\theta \cos^2\theta + Q_{22}^j \cos^4\theta, \\ \overline{Q}_{55}^j &= Q_{55}^j \cos^2\theta. \end{aligned} \tag{21}$$

The terms involved in Eq. (21) would be obtained as [114, 120–123]

$$Q_{11}^j = Q_{22}^j = \frac{E^j}{1 - (\nu^j)^2}, \quad Q_{12}^j = Q_{21}^j = \frac{E^j \nu^j}{1 - (\nu^j)^2}, \quad Q_{44}^j = Q_{55}^j = Q_{66}^j = \frac{E^j}{2(1 + \nu^j)}.$$

Therefore, the face sheets are assumed as in-plane flexible and transversely rigid panels. Also, the core is assumed as an in-plane and transversely flexible layer. Finally, in this model, there are fifteen displacement unknowns: five unknowns for each face sheet and five unknowns for the core.

2.4 Compatibility equations

The compatibility conditions assuming perfect bonding between the core and the composite layers that can be defined as follows:

$$\begin{aligned} & u^c(z_c = -h_c/2) = u^b(z_b = h_b/2), \\ & v^c(z_c = -h_c/2) = v^b(z_b = h_b/2), \\ & w^c(z_c = -h_c/2) = w^b(z_p = h_b/2), \\ & u^c(z_c = h_c/2) = u^t(z_t = -h_t/2), \\ & v^c(z_c = h_c/2) = v^t(z_t = -h_t/2), \\ & w^c(z_c = h_c/2) = w^t(z_t = -h_t/2). \end{aligned} \tag{22}$$

2.5 Extended Hamilton's principle

For obtaining the governing equation and associated boundary conditions, we can apply extended Hamilton's principle as follows [24–26, 98, 124–126]:

$$\int_{t_1}^{t_2} (\delta U - \delta W) \mathrm{d}t = 0. \tag{23}$$

The components of strain energy can be expressed as below:

$$
\delta U=\frac{1}{2}\Big(\iiint_V \sigma^c_{mn}\delta\varepsilon^c_{mn}dV^c+\iiint_V \sigma^j_{mn}\delta\varepsilon^j_{mn}dV^j\Big)=
$$

$$
=\iint_A\left[\begin{array}{l}
N^c_{xx}\Big(\frac{\partial\delta u^c_0}{\partial x}-\frac{\delta w^c_0}{R_1}\Big)+M^c_{xx}\frac{\partial\delta\phi u^c_x}{\partial x}-P^c_{xx}c_1\left(\frac{\partial\delta\phi^c_x}{\partial x}+\frac{\partial^2\delta w^c_0}{\partial x^2}\right)\\
+N^c_{yy}\Big(\frac{\partial\delta v^c_0}{\partial y}-\frac{\delta w^c_0}{R_2}\Big)+M^c_{yy}\frac{\partial\delta\phi^c_x}{\partial y}-P^c_{yy}c_1\left(\frac{\partial\delta\phi^c_y}{\partial y}+\frac{\partial^2\delta w^c_0}{\partial y^2}\right)\\
+N^c_{xy}\frac{\partial\delta u^c_0}{\partial y}+N^c_{xy}\frac{\partial\delta v^c_0}{\partial x}+M^c_{xy}\left(\frac{\partial\delta\phi^c_x}{\partial y}+\frac{\partial\delta\phi^c_y}{\partial x}\right)\\
-P^c_{xy}c_1\left(\frac{\partial\delta\phi^c_x}{\partial y}+\frac{\partial\delta\phi^c_y}{\partial x}+2\frac{\partial^2\delta w^c_0}{\partial x\partial y}\right)\\
+(Q^c_{xz}-3S^c_{xz}c_1)\left(\delta\phi^c_x+\frac{\partial\delta w^c_0}{\partial x}\right)+(Q^c_{yz}-3S^c_{yz}c_1)\left(\delta\phi^c_y+\frac{\partial\delta w^c_0}{\partial y}\right)
\end{array}\right](1+\frac{z^c}{R_1})(1+\frac{z^c}{R_2})dA^c+
$$

$$
\iint_A\left[\begin{array}{l}
N^j_{xx}\Big(\frac{\partial\delta u^j_0}{\partial x}-\frac{\delta w^j_0}{R_1}\Big)+M^j_{xx}\frac{\partial\delta\phi^j_x}{\partial x}-P^j_{xx}c_1\left(\frac{\partial\delta\phi^j_x}{\partial x}+\frac{\partial^2\delta w^j_0}{\partial x^2}\right)\\
+N^j_{yy}\Big(\frac{\partial\delta v^j_0}{\partial y}-\frac{\delta w^j_0}{R_2}\Big)+M^j_{yy}\frac{\partial\delta\phi^j_x}{\partial y}-P^j_{yy}c_1\left(\frac{\partial\delta\phi^j_y}{\partial y}+\frac{\partial^2\delta w^j_0}{\partial y^2}\right)\\
+N^j_{xy}\frac{\partial\delta u^j_0}{\partial y}+N^j_{xy}\frac{\partial\delta v^j_0}{\partial x}+M^j_{xy}\left(\frac{\partial\delta\phi^j_x}{\partial y}+\frac{\partial\delta\phi^j_y}{\partial x}\right)\\
-P^j_{xy}c_1\left(\frac{\partial\delta\phi^j_x}{\partial y}+\frac{\partial\delta\phi^j_y}{\partial x}+2\frac{\partial^2\delta w_0}{\partial x\partial y}\right)\\
+(Q^j_{xz}-3S^j_{xz}c_1)\left(\delta\phi^j_x+\frac{\partial\delta w^j_0}{\partial x}\right)+(Q^j_{yz}-3S^j_{yz}c_1)\left(\delta\phi^j_y+\frac{\partial\delta w^j_0}{\partial y}\right)
\end{array}\right](1+\frac{z^j}{R_1})(1+\frac{z^j}{R_2})dA^j, \tag{24a}
$$

which

$$
\begin{aligned}
&\left\{N^\lambda_{xx},N^\lambda_{yy},N^\lambda_{xy}\right\}=\int_{z_\lambda}\left\{\sigma^\lambda_{xx},\sigma^\lambda_{yy},\sigma^\lambda_{xy}\right\}dz_\lambda,\\
&\left\{M^\lambda_{xx},M^\lambda_{yy},M^\lambda_{xy}\right\}=\int_{z_\lambda}\left\{\sigma^\lambda_{xx},\sigma^\lambda_{yy},\sigma^\lambda_{xy}\right\}z_\lambda dz_\lambda,\\
&\left\{P^\lambda_{xx},P^\lambda_{yy},P^\lambda_{xy}\right\}=\int_{z_\lambda}\left\{\sigma^\lambda_{xx},\sigma^\lambda_{yy},\sigma^\lambda_{xy}\right\}z^3_\lambda dz_\lambda,\\
&\left\{Q^\lambda_{xz},Q^\lambda_{yz}\right\}=\int_{z_\lambda}\left\{\sigma^\lambda_{xz},\sigma^\lambda_{xy}\right\}dz_\lambda,\\
&\left\{S^\lambda_{xz},S^\lambda_{yz}\right\}=\int_{z_\lambda}\left\{\sigma^\lambda_{xz},\sigma^\lambda_{xy}\right\}z^2_\lambda dz_\lambda.
\end{aligned} \tag{24b}
$$

where $\lambda = b,\ t,\ c$.

Also, the kinetic energy [4–6, 8, 127–132] of each layer of the structure can be defined as bellow:

$$\begin{aligned}\delta K = &\int_{Z^j}\iint_{A^j}\rho^j\left\{\left(\frac{\partial u^j}{\partial t}\frac{\partial\delta u^j}{\partial t}\right)+\frac{\partial v^j}{\partial t}\frac{\partial\delta v^j}{\partial t}+\frac{\partial w^j}{\partial t}\frac{\partial\delta w^j}{\partial t}\right\}\left(1+\frac{z^j}{R_1}\right)\left(1+\frac{z^j}{R_2}\right)dA^j\\&+\int_{Z^c}\iint_{A^c}\rho^c\left\{\left(\frac{\partial u^c}{\partial t}\frac{\partial\delta u^c}{\partial t}\right)+\frac{\partial v^c}{\partial t}\frac{\partial\delta v^c}{\partial t}+\frac{\partial w^c}{\partial t}\frac{\partial\delta w^c}{\partial t}\right\}\left(1+\frac{z^c}{R_1}\right)\left(1+\frac{z^c}{R_2}\right)dA^c.\end{aligned}\tag{25}$$

Finally, the motion equations are derived as follows:

$$\begin{aligned}
&\delta u_0^c:\ \frac{\partial N_{xx}^c}{\partial x}+\frac{\partial N_{xy}^c}{\partial y}=I_0^c\frac{\partial^2u_0^c}{\partial t^2}+I_1^c\frac{\partial^2\phi_x^c}{\partial t^2}-I_3^cc_1\left(\frac{\partial^2\phi_x^c}{\partial t^2}+\frac{\partial^3w_0^c}{\partial t^2\partial x}\right),\\
&\delta v_0^c:\ \frac{\partial N_{yy}^c}{\partial y}+\frac{\partial N_{xy}^c}{\partial x}=I_0^c\frac{\partial^2v_0^c}{\partial t^2}+I_1^c\frac{\partial^2\phi_y^c}{\partial t^2}-I_3^cc_1\left(\frac{\partial^2\phi_y^c}{\partial t^2}+\frac{\partial^3w_0^c}{\partial t^2\partial y}\right),\\
&\delta w_0^c:\ c_1\frac{\partial^2P_{xx}^c}{\partial x^2}+c_1\frac{\partial^2P_{yy}^c}{\partial y^2}+2c_1\frac{\partial^2P_{xy}^c}{\partial x\partial y}+\frac{\partial Q_{xz}^c}{\partial x}-3c_1\frac{\partial S_{xz}^c}{\partial x}+\frac{\partial Q_{yz}^c}{\partial y}-3c_1\frac{\partial S_{yz}^c}{\partial y}\\
&+\frac{N_{xx}^c}{R_1}+\frac{N_{yy}^c}{R_2}=c_1I_3^c\frac{\partial^3u_0}{\partial x\partial t^2}+c_1I_4^c\frac{\partial^3\phi_x^c}{\partial x\partial t^2}-I_6^cc_1^2\left(\frac{\partial^3\phi_x^c}{\partial x\partial t^2}+\frac{\partial^4w_0^c}{\partial t^2\partial x^2}\right)\\
&+c_1I_3^c\frac{\partial^3v_y^c}{\partial y\partial t^2}+c_1I_3^c\frac{\partial^3\phi_y^c}{\partial y\partial t^2}-I_6^cc_1^2\left(\frac{\partial^3\phi_y^c}{\partial y\partial t^2}+\frac{\partial^4w_0^c}{\partial t^2\partial y^2}\right)+\left(I_0^c\frac{\partial^2w_0^c}{\partial t^2}\right),\\
&\delta\phi_x^c:\ \frac{\partial M_{xx}^c}{\partial x}-c_1\frac{\partial P_{xx}^c}{\partial x}+\frac{\partial M_{xy}^c}{\partial y}-c_1\frac{\partial P_{xy}^c}{\partial y}-Q_{xz}^c+3c_1S_{xz}^c=\\
&+I_1^c\frac{\partial^2u_0}{\partial t^2}+I_2^c\frac{\partial^2\phi_x}{\partial t^2}-I_4^cc_1\left(\frac{\partial^2\phi_x}{\partial t^2}+\frac{\partial^3w}{\partial t^2\partial x}\right)\\
&-c_1I_3^c\frac{\partial^2u_0}{\partial t^2}-c_1I_4^c\frac{\partial^2\phi_x}{\partial t^2}+I_6^cc_1^2\left(\frac{\partial^2\phi_x^c}{\partial t^2}+\frac{\partial^3w_0^c}{\partial t^2\partial x}\right),\\
&\delta\phi_y^c:\ \frac{\partial M_{yy}^c}{\partial y}-c_1\frac{\partial P_{yy}^c}{\partial y}+\frac{\partial M_{xy}^c}{\partial x}-c_1\frac{\partial P_{xy}^c}{\partial x}-Q_{yz}^c+3c_1S_{yz}^c=\\
&I_1^c\frac{\partial^2v_0}{\partial t^2}+I_2^c\frac{\partial^2\phi_y}{\partial t^2}-I_4^cc_1\left(\frac{\partial^2\phi_y^c}{\partial t^2}+\frac{\partial^3w_0^c}{\partial t^2\partial y}\right)\\
&-c_1I_3^c\frac{\partial^2v_0}{\partial t^2}-c_1I_4^c\frac{\partial^2\phi_y}{\partial t^2}+I_6^cc_1^2\left(\frac{\partial^2\phi_y^c}{\partial t^2}+\frac{\partial^3w_0^c}{\partial t^2\partial y}\right).
\end{aligned}\tag{26}$$

Also, the motion equations for the nanocomposite face sheets are as follows:

$$
\begin{aligned}
&\delta u_0^j : \frac{\partial N_{xx}^j}{\partial x} + \frac{\partial N_{xy}^j}{\partial y} = I_0^j \frac{\partial^2 u_0^j}{\partial t^2} + I_1^j \frac{\partial^2 \phi_x^j}{\partial t^2} - I_3^j c_1 \left(\frac{\partial^2 \phi_x^j}{\partial t^2} + \frac{\partial^3 w_0^j}{\partial t^2 \partial x} \right), \\
&\delta v_0^j : \frac{\partial N_{yy}^j}{\partial y} + \frac{\partial N_{xy}^j}{\partial x} = I_0^j \frac{\partial^2 v_0^j}{\partial t^2} + I_1^j \frac{\partial^2 \phi_y^j}{\partial t^2} - I_3^j c_1 \left(\frac{\partial^2 \phi_y^j}{\partial t^2} + \frac{\partial^3 w_0^j}{\partial t^2 \partial y} \right), \\
&\delta w_0^j : c_1 \frac{\partial^2 P_{xx}^j}{\partial x^2} + c_1 \frac{\partial^2 P_{yy}^j}{\partial y^2} + 2c_1 \frac{\partial^2 P_{xy}^j}{\partial x \partial y} + \frac{\partial Q_{xz}^j}{\partial x} - 3c_1 \frac{\partial S_{xz}^j}{\partial x} + \frac{\partial Q_{yz}^j}{\partial y} - 3c_1 \frac{\partial S_{yz}^j}{\partial y} \\
&+ \frac{N_{xx}^j}{R_1} + \frac{N_{yy}^j}{R_2} = c_1 I_3^j \frac{\partial^3 u_0^j}{\partial x \partial t^2} + c_1 I_4^j \frac{\partial^3 \phi_x^j}{\partial x \partial t^2} - I_6^j c_1^2 \left(\frac{\partial^3 \phi_x^j}{\partial x \partial t^2} + \frac{\partial^4 w_0^j}{\partial t^2 \partial x^2} \right) \\
&+ c_1 I_3^j \frac{\partial^3 v_0^j}{\partial y \partial t^2} + c_1 I_4^j \frac{\partial^3 \phi_y^j}{\partial y \partial t^2} - I_6^j c_1^2 \left(\frac{\partial^3 \phi_y^j}{\partial y \partial t^2} + \frac{\partial^4 w_0^j}{\partial t^2 \partial y^2} \right) + \left(I_0^j \frac{\partial^2 w_0^j}{\partial t^2} \right), \\
&\delta \phi_x^j : \frac{\partial M_{xx}^j}{\partial x} - c_1 \frac{\partial P_{xx}^j}{\partial x} + \frac{\partial M_{xy}^j}{\partial y} - c_1 \frac{\partial P_{xy}^j}{\partial y} - Q_{xz}^j + 3c_1 S_{xz}^j = \\
&+ I_1^j \frac{\partial^2 u_0^j}{\partial t^2} + I_2^j \frac{\partial^2 \phi_x^j}{\partial t^2} - I_4^j c_1 \left(\frac{\partial^2 \phi_x^j}{\partial t^2} + \frac{\partial^3 w_0^j}{\partial t^2 \partial x} \right) \\
&- c_1 I_3^j \frac{\partial^2 u_0^j}{\partial t^2} - c_1 I_4^j \frac{\partial^2 \phi_x^j}{\partial t^2} + I_6^j c_1^2 \left(\frac{\partial^2 \phi_x^j}{\partial t^2} + \frac{\partial^3 w_0^j}{\partial t^2 \partial x} \right), \\
&\delta \phi_y^j : \frac{\partial M_{yy}^j}{\partial y} - c_1 \frac{\partial P_{yy}^j}{\partial y} + \frac{\partial M_{xy}^j}{\partial x} - c_1 \frac{\partial P_{xy}^j}{\partial x} - Q_{yz}^j + 3c_1 S_{yz}^j = \\
&I_1^j \frac{\partial^2 v_0^j}{\partial t^2} + I_2^j \frac{\partial^2 \phi_y^j}{\partial t^2} - I_4^j c_1 \left(\frac{\partial^2 \phi_y^j}{\partial t^2} + \frac{\partial^3 w_0^j}{\partial t^2 \partial y} \right) \\
&- c_1 I_3 \frac{\partial^2 v_0^j}{\partial t^2} - c_1 I_4 \frac{\partial^2 \phi_y^j}{\partial t^2} + I_6 c_1^2 \left(\frac{\partial^2 \phi_y^j}{\partial t^2} + \frac{\partial^3 w_0^j}{\partial t^2 \partial y} \right).
\end{aligned} \tag{27}
$$

It is worth mentioning that, according to compatibility equations (Eq. 22), the numbers of unknown variables are decreased from 15 to 9. Therefore, the total number of unknowns in the core and the face sheet is reduced to 9.

2.6 Solution procedure

Displacement fields for investigation the wave propagation analysis of the structure defined as follow [24–26, 109]:

$$
\begin{Bmatrix} u_0^c \\ v_0^c \\ w_0^c \\ \phi_x^c \\ \phi_y^c \end{Bmatrix} = \begin{Bmatrix} U_0^c \exp(sx + n\theta - \omega t)i \\ V_0^c \exp(sx + n\theta - \omega t)i \\ W_0^c \exp(sx + n\theta - \omega t)i \\ \Phi_x^c \exp(sx + n\theta - \omega t)i \\ \Phi_y^c \exp(sx + n\theta - \omega t)i \end{Bmatrix}, \quad \begin{Bmatrix} u_0^j \\ v_0^j \\ w_0^j \\ \phi_x^j \\ \phi_y^j \end{Bmatrix} = \begin{Bmatrix} U_0^j \exp(sx + n\theta - \omega t)i \\ V_0^j \exp(sx + n\theta - \omega t)i \\ W_0^j \exp(sx + n\theta - \omega t)i \\ \Phi_x^j \exp(sx + n\theta - \omega t)i \\ \Phi_y^j \exp(sx + n\theta - \omega t)i \end{Bmatrix}. \tag{28}
$$

where s and n are wave number along with the directions of x and y, respectively, also ω is called frequency. With replacing Eq. (28) into governing equations achieve to [133–137]:

$$
([K] - \omega^2 [M])\{d\} = \{0\}, \tag{29}
$$

where

$$
\{d\} = \left\{ u_0 \;\; v_0 \;\; w_0 \;\; \psi_{x_0} \;\; \psi_{\theta_0} \right\}. \tag{30}
$$

Also, the phase velocity of wave dispersion can be calculated by Eq. (29):

$$
c = \frac{\omega}{s}. \tag{31}
$$

In the Eq. (31), c and s are called phase velocity and wavenumber of a laminated nanocomposite cylindrical shell. These parameters are propagation speeds of the particles in a sandwich panel.

2.7 Validation

The obtained results for the perfect panel are compared with the results of Refs.[138, 139]. These results are listed in Table 1 and 2. From these tables, it can be seen that the present results have a good agreement with the obtained results in the literature. Note that, the dimensionless form of the frequency can be calculated using the below relation:

$$\Omega = \omega \frac{a^2}{h}\sqrt{\frac{\rho_M}{E_M}}. \tag{32}$$

For more verification, the fundamental frequencies of the FML moderately thick plates resting on partial elastic foundations are calculated by the free vibration Eq. (21) as an eigenvalue problem. In Table 2, non-dimensional fundamental frequencies of the symmetrically laminated cross-ply plate $(0^\circ, 90^\circ, 90^\circ, 0^\circ)$ are shown as compared for different E_1/E_2.

3 Results

In this part, a comprehensive investigation is carried out to demonstrate the effects of various parameters on the phase velocity response of a multi-hybrid nanocomposite doubly curved panel. The geometrical and material characteristics of constituent materials would be presented in Table 3.

With pay attention to Fig. 1 can find an investigation about the impacts of the various CNTs weight fraction (W_{CNT}) and core to total thickness ratio (h_c/h) of the FML panel on the wave responses of the doubly carved panel.

As stated by Fig. 2, the impact of W_{CNT} on the phase velocity is obvious and considerable if the h_c/h is less than 0.8. in another word for $0 \le h_c/h \le 0.8$, the phase velocity can improve due to increasing the CNTs' weight fraction and this enhancement will be weakened by increasing the core thickness of the FML panel. Also, when the thickness of the core is small, the phase velocity falling down owning to increasing the h_c/h, but if we consider the thicker core, we can find an indirect relation between h_c/h and phase velocity. Accordingly, the sensitivity of the phase velocity of the FML panel to the W_{CNT} can decrease when we consider the core of the panel thicker.

From Fig. 3, we can find research about the effects of the various FG face sheet patterns and core to total thickness ratio (h_c/h) of the FML panel on the wave responses of the MHC reinforced doubly carved panel.

The most obvious result in Fig. 3 is that for having an impact from FG face sheet patterns on the phase velocity we should consider the h_c/h less than 0.2. As another explanation, considering different FG face sheet patterns will be ineffective at the higher value of the h_c/h. As a practical result, according to Fig. 3, it can be stated that the sensitivity of the phase velocity of the FML panel to the different FG face sheet patterns can decrease when the thickness of the core of the FML panel increases. Generally, for each h_c/h, when the face sheet is made by Pattern 1 and Pattern 3, we can see the lowest and highest phase velocity in the sandwich panel.

With the aid of Fig. 4, presented the effects of the wavenumber and small radius to total thickness ratio (R_1/h) of the FML panel on the wave responses of the FML reinforced doubly carved panel.

The most evident outcome in Fig. 4 is that boosting the wave number can be an encouragement for improving the phase velocity of the FML panel and this impact from wavenumber on the wave propagation of the sandwich structure will change to be ineffective when the wavenumber is more than 11e4. As a practical result, if the small radius of the FML doubly curved panel is rising, the phase velocity of the system can increase and this impact will be ineffectual at the higher value of the wavenumber.

With attention to Fig. 5 can see an investigation for analysis the impacts of the various CNTs weight fraction (W_{CNT}) and wavenumber on the wave responses of the FML doubly carved panel.

The apparent and the most important result in Fig. 5 is that if there is more distribution of CNTs in the matrix of

Table 1 Comparison of the first dimensionless natural frequency of simply supported CNT reinforced composite square perfect panel (a/h = 10)

V_{CNT}	Ref [138]	Ref [139]	Present study
11%	0.1319	0.1357	0.1350
14%	0.1400	0.1438	0.1429
17%	0.1638	0.1685	0.1658

Table 2 Non-dimensional fundamental frequency of SSSS cross-ply laminated square plate with $G_{12}/E_2 = 0.6$, $G_{13}/E_2 = 0.6$, $G_{23}/E_2 = 0.5$, $a = b = 1$, $\upsilon = 0.25$

E_1/E_2	Ref [140]	Ref [141]	Presented study	Discrepancy
10	8.2982	8.2981	8.5485	3%
20	9.5671	9.5671	10.0328	4%
30	10.326	10.326	10.6318	2%
40	10.824	10.854	11.0045	1%

Table 3 Material properties of the multiscale hybrid nanocomposite annular plate [122]

Carbon fiber	E_{11}^{F}	E_{22}^{F}	G_{12}^{F}	ρ^{F}	ν^{F}	α_{11}^{F}	α_{22}^{F}		
	[Gpa]	[Gpa]	[Gpa]	[kg/m^3]		[$\times10^{-6}$/k]	[$\times10^{-6}$/k]		
	233.05	23.1	8.96	1750	0.2	−0.54	10.08		
Epoxy matrix	E^{m}	ν^{m}	ρ^{m}	α^{m}					
	[Gpa]		[kg/m^3]	[$\times10^{-6}$/k]					
	3.51	0.34	1200	45					
Carbon nanotube	E_{11}^{F}	$E_{22}^{CNT}=E_{33}^{CNT}$	$G_{12}^{CNT}=G_{13}^{CNT}$	ν_{12}^{CNT}	ρ^{CNT}	α^{CNT}	l^{CNT}	d^{CNT}	t^{CNT}
	[Tpa]	[Tpa]	[Tpa]		[kg/m^3]	[$\times10^{-6}$/k]	[μm]	[nm]	[nm]
	5.6466	7.0800	1.9445	0.175	1350	3.4584	25	1.4	0.34

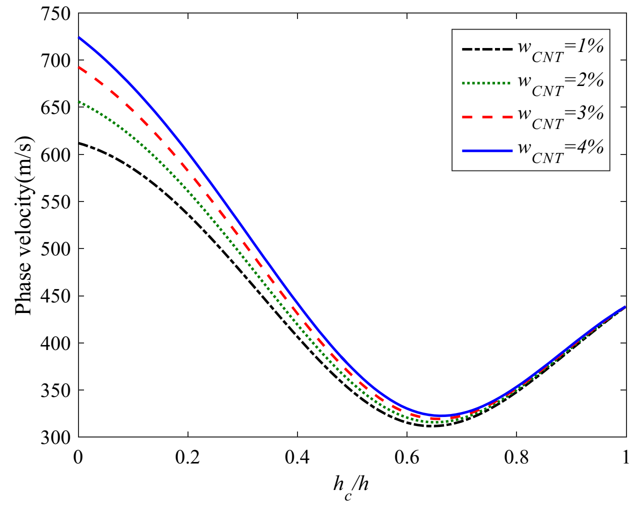

Fig. 2 Phase velocity versus h_c/h with having attention to the impact of W_{CNT}

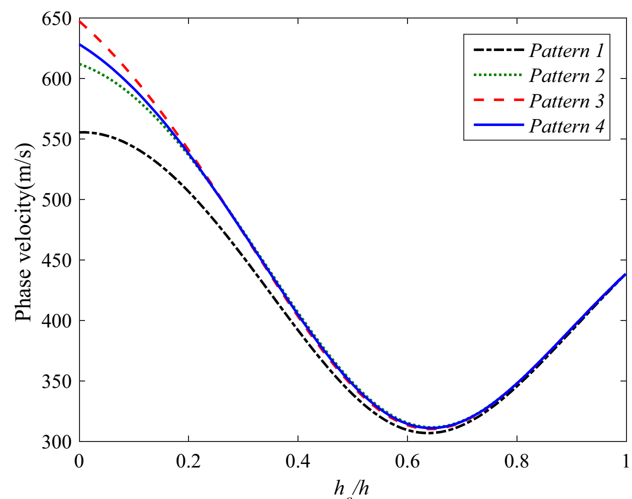

Fig. 3 Phase velocity versus h_c/h with having attention to the impact of different FG face sheet patterns

the face sheet of the FML panel, we will find that the phase velocity or wave response of the system can improve and without a doubt, this issue is considerable at the higher wavenumber.

Presented diagrams in Fig. 6 are drawn to have an explanation about the effects of the wavenumber and different FG face sheet patterns of the FML panel on the wave responses of the FML reinforced doubly carved panel.

The bolded result in Fig. 6 is that boosting the wave number can be an encouragement for improving the phase velocity of the FML panel and this impact from wavenumber on the wave propagation of the sandwich structure will change

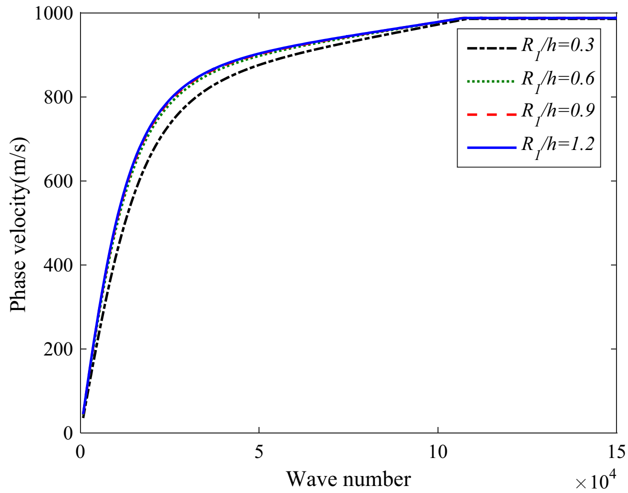

Fig. 4 Phase velocity versus wavenumber by having attention to the impact of R_1/h

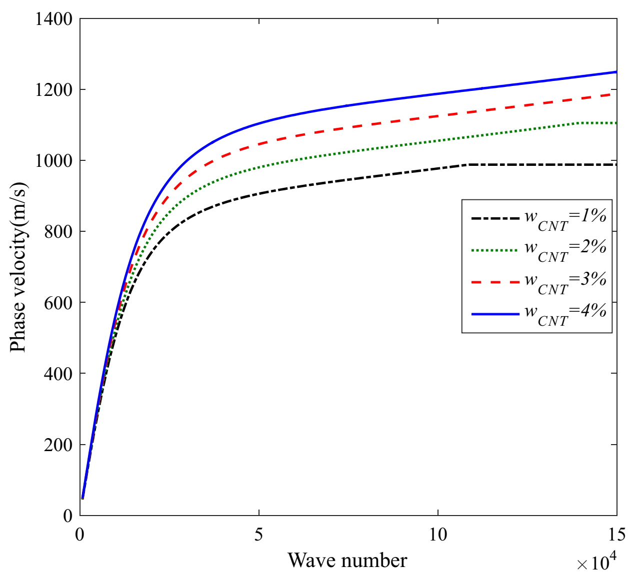

Fig. 5 Phase velocity versus wavenumber by having attention to the impact of W_{CNT}

to be ineffective in the higher value of the wavenumber. As a practical result and at the lower wavenumber, when the face sheet is made by Pattern 1 and Pattern 3, we can see the lowest and highest phase velocity in the sandwich panel. Also, the wave propagation response of the FML panel with Pattern 2, 3, and 4 is similar when the wavenumber is great enough.

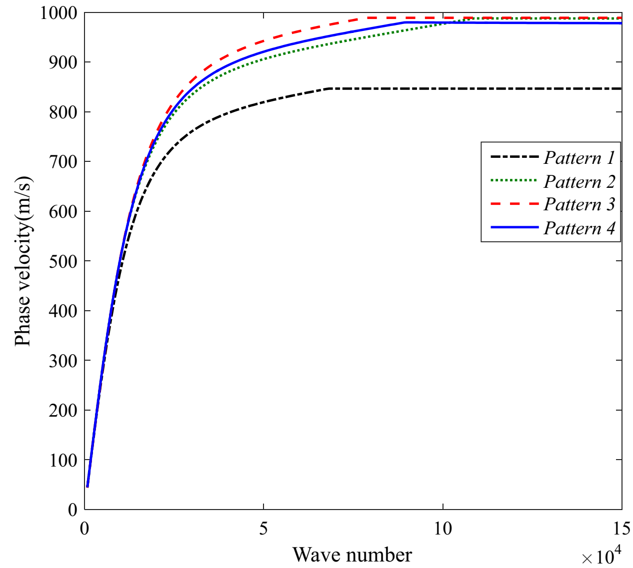

Fig. 6 Phase velocity versus wavenumber by having attention to the impact of different FG face sheet patterns

With the aid of Fig. 7, the effects of the fibers angel and different FG face sheet patterns on the wave responses of the FML reinforced doubly carved panel are presented.

The most general result in Fig. 7 is that for each FG face sheet patterns when the fibers angel is less than $\pi/2$, the phase velocity is decreasing and this trend will be revers for the fibers angel more than $\pi/2$. As the most interesting result from Fig. 7 is that when the fiber angel is $0.3 \leq \theta/\pi \leq 0.7$, employing different FG patterns for making the FML cannot provide any change on the phase velocity of the structure. As another explanation, if the fibers are distributed in the matrix vertically, changing the FG patterns cannot play any roles on the wave response of the FML panel and as the fibers become horizontal, the effect of the FG patterns on the phase velocity becomes more dramatic. Reported data in Fig. 8 are shown to have a deep presentation about the effects of the wavenumber, fibers angel of the FML panel, and small radius to total thickness ratio (R_1/h) of the FML panel on the wave responses of the doubly carved panel.

If we have excellent attention to Fig. 8, it could be seen that within a certain range of the core to total thickness ratio, there is no effect from the small radius to total thickness ratio of the FML panel on the phase velocity, and this range will be wider if the wave number rises. Also, for the lower wavenumber, when the fiber angel is 0 and 1 radians, the pick of the phase velocity of the system will happen but as the wave number increases, the maximum value of the phase velocity will be seen at 0.25 and 0.75 radians.

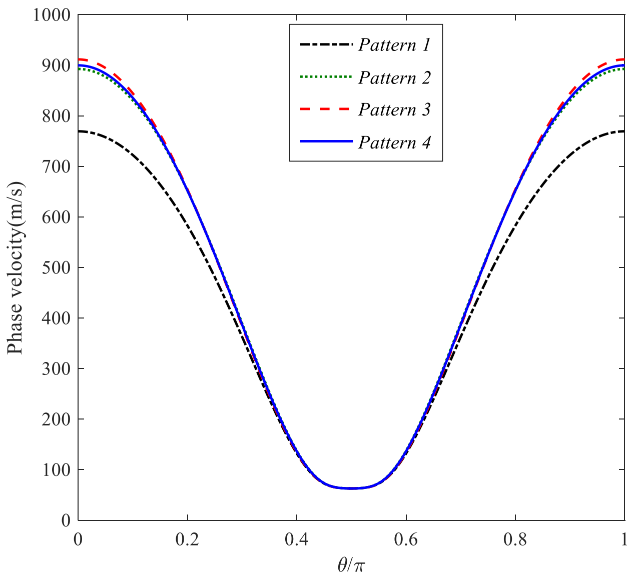

Fig. 7 Phase velocity versus fibers angel by having attention to the impact of different FG face sheet patterns

With the aid of Fig. 9, the effects of the fibers angel and weight fraction of CNTs (W_{CNT}) on the wave responses of the FML doubly carved panel are presented.

The most interesting result from Fig. 9 is that when the fiber angel is $0.4 \leq \theta/\pi \leq 0.6$, increasing W_{CNT} cannot provide any change on the phase velocity of the structure. As another explanation, if the fibers are distributed in the matrix vertically, changing the W_{CNT} cannot play any roles on the wave response of the FML panel and as the fibers become horizontal, the effect of W_{CNT} on the phase velocity becomes more dramatic. With pay attention to Fig. 10, we can see a study about the effects of the fibers angel and core to total thickness ratio (h_c/h) of the FML panel on the wave responses of the doubly carved panel.

as stated by Fig. 10 when the fiber angel is $0 \leq \theta/\pi \leq 0.42$ and $0.58 \leq \theta/\pi \leq 1$, the phase velocity will be improved by having each decline in the core to total thickness ratio but this relation between fiber angel and h_c/h change to direct as the fibers angel is $0.42 < \theta/\pi < 0.58$. The reported 3D diagram in Figs. 11 and 12 are shown to have a comparative study about the effects of the wavenumber, core to total thickness ratio (h_c/h) of the FML panel, and fiber angle on the wave responses of the doubly carved panel.

The most principal and evident result in Figs. 11 and 12 are that as the wave number increases, the changes in phase velocity of the MHC reinforced sandwich panel which is caused by increasing the fibers angel and core to total thickness ratio become much more dramatic. In the simpler word, the effects of fibers angel and core to total thickness ratio on the phase velocity of the FML panel are highly dependent on the wavenumber.

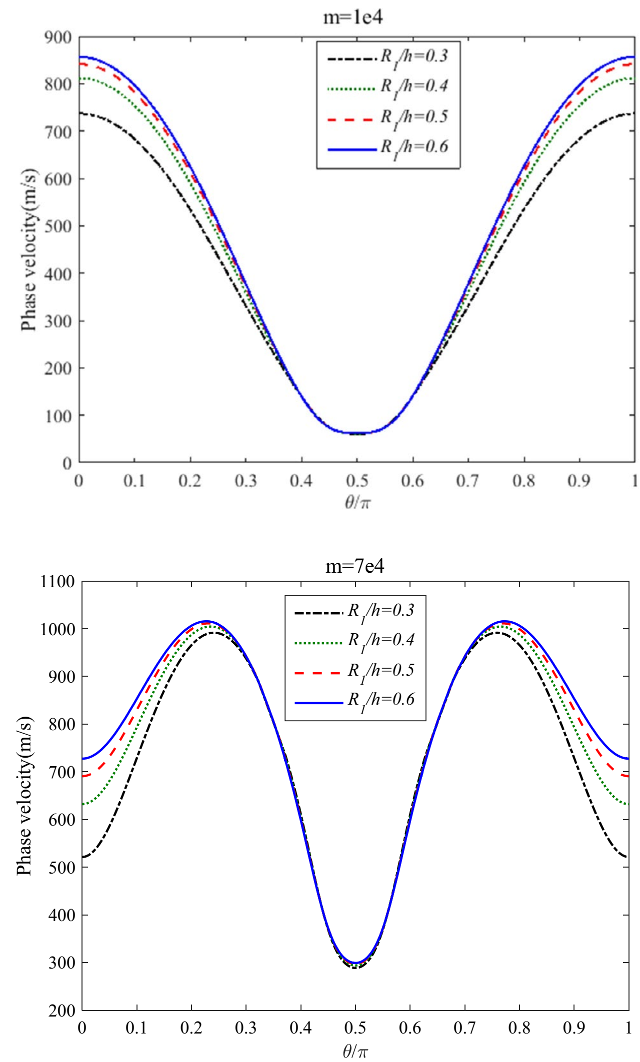

Fig. 8 Phase velocity versus fibers angel for two value of wavenumber

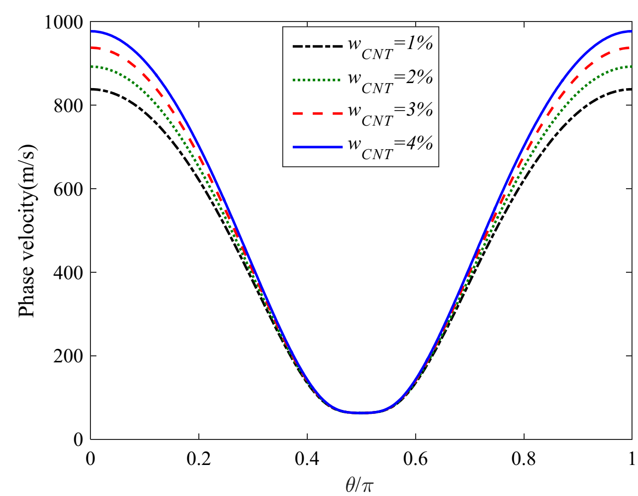

Fig. 9 Phase velocity versus θ/π for different value of W_{CNT}

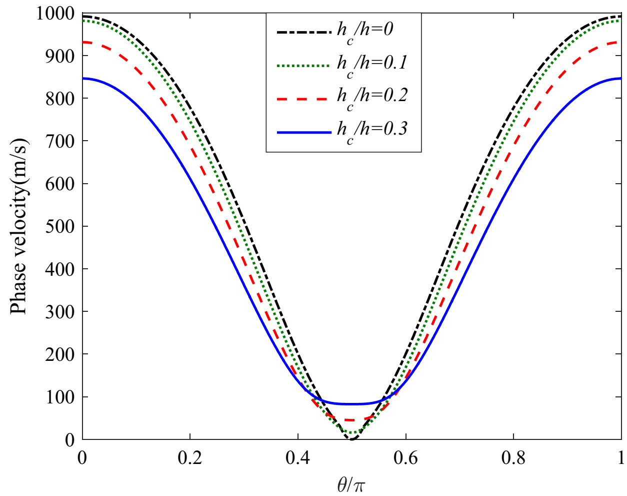

Fig. 10 Phase velocity versus θ/π for different value of h_c/h

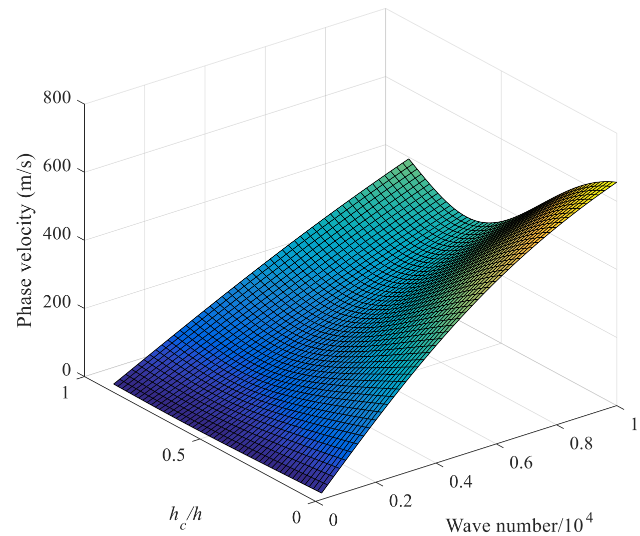

Fig. 12 Phase velocity of the FML panel by concerning the impacts of wavenumber and core to total thickness ratio

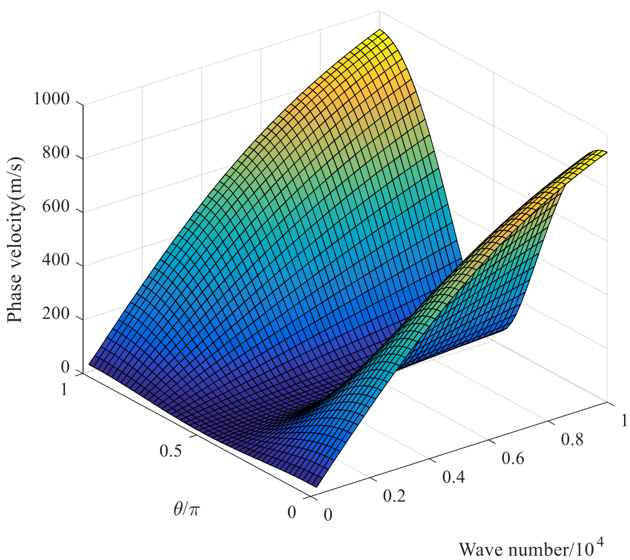

Fig. 11 Phase velocity of the FML panel with respects to the impact of wavenumber and fibers angel

4 Conclusion

Wave propagation characteristics of a sandwich structure with the soft core and multi-hybrid nanocomposite face sheets is investigated. The stresses and strains are obtained using HSDT. Rule of the mixture and modified Halpin–Tsai model are engaged to provide the effective material constant of the multi-hybrid nanocomposite face sheets of the sandwich panel. Via the compatibility rule, the bonding between the smart layer and a soft core is modeled. Finally, the most bolded results of this paper are as follow:

- it is true that when the thickness of the core is small, the phase velocity falling down owning to increasing the h_c/h, but if we consider the thicker core, we can find an indirect relation between h_c/h and phase velocity;
- the sensitivity of the phase velocity of the FML panel to the W_{CNT} and different FG face sheet patterns can decrease when we consider the core of the panel thicker;
- boosting the wave number can be an encouragement for improving the phase velocity of the FML panel and this impact from wavenumber on the wave propagation of the sandwich structure will change to be ineffective when the wavenumber is more than 11e4;
- as a practical result, if the small radius of the FML doubly curved panel is rising, the phase velocity of the system can increase and this impact will be ineffectual at the higher value of the wavenumber;
- if the fibers are distributed in the matrix vertically, changing the FG patterns cannot play any role on the wave response of the FML panel and as the fibers become horizontal, the effect of the FG patterns on the phase velocity becomes more dramatic;
- when the fiber angel is 0 and 1 radians, the pick of the phase velocity of the system will happen but as the wave number increases, the maximum value of the phase velocity will be seen at 0.25 and 0.75 radians;
- when the fiber angel is $0 \leq \theta/\pi \leq 0.42$ and $0.58 \leq \theta/\pi \leq 1$, the phase velocity will be improved by having each decline in the core to total thickness ratio but this relation between fiber angel and h_c/h changes to direct as the fiber angel is $0.42 < \theta/\pi < 0.58$;

- the effects of fibers angel and core to total thickness ratio on the phase velocity of the FML panel is hardly dependent on the wavenumber.

Funding National Natural Science Foundation of China (51675148). The Outstanding Young Teachers Fund of Hangzhou Dianzi University (GK160203201002/003). National Natural Science Foundation of China (51805475). This research was supported by the 2020 scientific promotion funded by Jeju National University.

References

1. Ghayesh MH (2018) Dynamics of functionally graded viscoelastic microbeams. Int J Eng Sci 124:115–131
2. Ghayesh MH (2019) Nonlinear oscillations of FG cantilevers. Appl Acoust 145:393–398
3. Ghayesh MH (2018) Nonlinear vibration analysis of axially functionally graded shear-deformable tapered beams. Appl Math Model 59:583–596
4. Ghabussi A, Habibi M, NoormohammadiArani O, Shavalipour A, Moayedi H, Safarpour H (2020) Frequency characteristics of a viscoelastic graphene nanoplatelet–reinforced composite circular microplate. J Vib Control 1:1077546320923930
5. Safarpour M, Ghabussi A, Ebrahimi F, Habibi M, Safarpour H (2020) Frequency characteristics of FG-GPLRC viscoelastic thick annular plate with the aid of GDQM. Thin-Walled Struct 150:106683
6. Cheshmeh E, Karbon M, Eyvazian A, Jung D, Tran T, Habibi M et al Buckling and vibration analysis of FG-CNTRC plate subjected to thermo-mechanical load based on higher-order shear deformation theory. Mech Based Des Struct Mach
7. Shariati A, Mohammad-Sedighi H, Żur KK, Habibi M, Safa M (2020) Stability and dynamics of viscoelastic moving Rayleigh beams with an asymmetrical distribution of material parameters. Symmetry 12:586
8. Oyarhossein MA, Alizadeh AA, Habibi M, Makkiabadi M, Daman M, Safarpour H et al (2020) Dynamic response of the nonlocal strain-stress gradient in laminated polymer composites microtubes. Sci Rep 10:5616
9. Habibi M, Taghdir A, Safarpour H (2019) Stability analysis of an electrically cylindrical nanoshell reinforced with graphene nanoplatelets. Compos B Eng 175:107125
10. Chen S, Hassanzadeh-Aghdam M, Ansari R (2018) An analytical model for elastic modulus calculation of SiC whisker-reinforced hybrid metal matrix nanocomposite containing SiC nanoparticles. J Alloy Compd 767:632–641
11. Ebrahimi F, Habibi M, Safarpour H (2019) On modeling of wave propagation in a thermally affected GNP-reinforced imperfect nanocomposite shell. Eng Comput 35:1375–1389
12. Li C, Han Q (2020) Analyzing wave propagation in graphene-reinforced nanocomposite annular plates by the semi-analytical formulation. Mech Adv Mater Struct 1:1–14
13. Aminipour H, Janghorban M, Li L (2020) Wave dispersion in nonlocal anisotropic macro/nanoplates made of functionally graded materials. Waves Random Complex Media 1:1–45
14. Zhang X, Zhang Y, Liu Z, Liu J (2020) Analysis of heat transfer and flow characteristics in typical cambered ducts. Int J Therm Sci 150:106226
15. Hu X, Ma P, Wang J, Tan G (2019) A hybrid cascaded DC–DC boost converter with ripple reduction and large conversion ratio. IEEE J Emerg Sel Top Power Electron 8:761–770
16. Hu X, Ma P, Gao B, Zhang M (2019) An integrated step-up inverter without transformer and leakage current for grid-connected photovoltaic system. IEEE Trans Power Electron 34:9814–9827
17. Wu X, Huang B, Wang Q, Wang Y (2020) High energy density of two-dimensional MXene/NiCo-LDHs interstratification assembly electrode: understanding the role of interlayer ions and hydration. Chem Eng J 380:122456
18. Guo L, Sriyakul T, Nojavan S, Jermsittiparsert K (2020) Risk-based traded demand response between consumers' aggregator and retailer using downside risk constraints technique. IEEE Access 8:90957–90968
19. Cao B, Zhao J, Lv Z, Gu Y, Yang P, Halgamuge SK (2020) Multiobjective evolution of fuzzy rough neural network via distributed parallelism for stock prediction. IEEE Trans Fuzzy Syst 28:939–952
20. Wang G, Yao Y, Chen Z, Hu P (2019) Thermodynamic and optical analyses of a hybrid solar CPV/T system with high solar concentrating uniformity based on spectral beam splitting technology. Energy 166:256–266
21. Liu Y, Yang C, Sun Q (2020) Thresholds based image extraction schemes in big data environment in intelligent traffic management. IEEE Trans Intell Transport Syst
22. Liu J, Liu Y, Wang X (2019) An environmental assessment model of construction and demolition waste based on system dynamics: a case study in Guangzhou. Environ Sci Pollut Res 31:1–23
23. Xu W, Qu S, Zhao L, Zhang H (2020) An improved adaptive sliding mode observer for a middle and high-speed rotors tracking. In: IEEE transactions on power electronics
24. Nadri S, Xie L, Jafari M, Bauwens MF, Arsenovic A, Weikle RM (2019) Measurement and extraction of parasitic parameters of quasi-vertical schottky diodes at submillimeter wavelengths. IEEE Microwave Wirel Compon Lett 29:474–476
25. Nadri S, Xie L, Jafari M, Alijabbari N, Cyberey ME, Barker NS et al (2018) A 160 GHz frequency quadrupler based on heterogeneous integration of GaAs Schottky diodes onto silicon using SU-8 for epitaxy transfer. IEEE/MTT-S Int Microwave Sympos-IMS 2018:769–772
26. Weikle RM, Xie L, Nadri S, Jafari M, Moore CM, Alijabbari N et al (2019) Submillimeter-wave Schottky diodes based on heterogeneous integration of GaAs onto silicon. In: 2019 United States National Committee of URSI National Radio Science Meeting (USNC-URSI NRSM), pp 1–2
27. Cao L, Tu C, Hu P, Liu S (2019) Influence of solid particle erosion (SPE) on safety and economy of steam turbines. Appl Therm Eng 150:552–563
28. Wang Y, Cao L, Hu P, Li B, Li Y (2019) Model establishment and performance evaluation of a modified regenerative system for a 660 MW supercritical unit running at the IPT-setting mode. Energy 179:890–915
29. Zhu B, Zhou X, Liu X, Wang H, He K, Wang P (2020) Exploring the risk spillover effects among China's pilot carbon markets: a regular vine copula-CoES approach. J Clean Product 242:118455
30. Liu X, Zhou X, Zhu B, He K, Wang P (2019) Measuring the maturity of carbon market in China: an entropy-based TOPSIS approach. J Clean Product 229:94–103
31. Zhu B, Ye S, Jiang M, Wang P, Wu Z, Xie R et al (2019) Achieving the carbon intensity target of China: a least squares support vector machine with mixture kernel function approach. Appl Energy 233:196–207

32. Zhu B, Su B, Li Y (2018) Input-output and structural decomposition analysis of India's carbon emissions and intensity, 2007/08–2013/14. Appl Energy 230:1545–1556
33. Cao Y, Li Y, Zhang G, Jermsittiparsert K, Nasseri M (2020) An efficient terminal voltage control for PEMFC based on an improved version of whale optimization algorithm. Energy Rep 6:530–542
34. Liu Y-X, Yang C-N, Sun Q-D, Wu S-Y, Lin S-S, Chou Y-S (2019) Enhanced embedding capacity for the SMSD-based data-hiding method. Signal Process Image Commun 78:216–222
35. Quan Q, Hao Z, Xifeng H, Jingchun L (2020) Research on water temperature prediction based on improved support vector regression. Neural Comput Appl 1:1–10
36. Ebrahimi F, Sedighi SB (2020) Wave dispersion characteristics of a rectangular sandwich composite plate with tunable magneto-rheological fluid core rested on a visco-Pasternak foundation. Mech Based Des Struct Mach 1–14
37. Faroughi S, Rahmani A, Friswell M (2020) On wave propagation in two-dimensional functionally graded porous rotating nano-beams using a general nonlocal higher-order beam model. Appl Math Model 80:169–190
38. Liu C, Yu J, Xu W, Zhang X, Zhang B (2020) Theoretical study of elastic wave propagation through a functionally graded micro-structured plate base on the modified couple-stress theory. Meccanica 1–15
39. Ebrahimi F, Barati MR, Haghi P (2017) Thermal effects on wave propagation characteristics of rotating strain gradient temperature-dependent functionally graded nanoscale beams. J Therm Stresses 40:535–547
40. Barati MR (2017) On wave propagation in nanoporous materials. Int J Eng Sci 116:1–11
41. Gao W, Qin Z, Chu F (2020) Wave propagation in functionally graded porous plates reinforced with graphene platelets. Aerosp Sci Technol 105860
42. Ebrahimi F, Barati MR, Dabbagh A (2016) A nonlocal strain gradient theory for wave propagation analysis in temperature-dependent inhomogeneous nanoplates. Int J Eng Sci 107:169–182
43. Safaei B, Moradi-Dastjerdi R, Qin Z, Behdinan K, Chu F (2019) Determination of thermoelastic stress wave propagation in nano-composite sandwich plates reinforced by clusters of carbon nano-tubes. J Sandwich Struct Mater 1099636219848282
44. Barati MR, Zenkour AM (2019) Analysis of postbuckling of graded porous GPL-reinforced beams with geometrical imperfection. Mech Adv Mater Struct 26:503–511
45. Shahverdi H, Barati MR, Hakimelahi B (2019) Post-buckling analysis of honeycomb core sandwich panels with geometrical imperfection and graphene reinforced nano-composite face sheets. Mater Res Express 6:095017
46. Barati MR, Shahverdi H (2020) Finite element forced vibration analysis of refined shear deformable nanocomposite graphene platelet-reinforced beams. J Braz Soc Mech Sci Eng 42:33
47. Mirjavadi SS, Forsat M, Hamouda A, Barati MR (2019) Dynamic response of functionally graded graphene nanoplatelet reinforced shells with porosity distributions under transverse dynamic loads. Mater Res Express 6:075045
48. Mirjavadi SS, Afshari BM, Barati MR, Hamouda A (2019) Nonlinear free and forced vibrations of graphene nanoplatelet reinforced microbeams with geometrical imperfection. Microsyst Technol 25:3137–3150
49. Barati MR, Zenkour AM (2019) Analysis of postbuckling behavior of general higher-order functionally graded nanoplates with geometrical imperfection considering porosity distributions. Mech Adv Mater Struct 26:1081–1088
50. Liu W, Zhang X, Li H, Chen J Investigation on the deformation and strength characteristics of rock salt under different confining pressures. Geotech Geol Eng 1–15
51. Eyvazian A, Hamouda AM, Tarlochan F, Mohsenizadeh S, Dastjerdi AA (2019) Damping and vibration response of viscoelastic smart sandwich plate reinforced with non-uniform graphene platelet with magnetorheological fluid core. Steel Compos Struct 33:891
52. Motezaker M, Eyvazian A (2020) Post-buckling analysis of mindlin cut out-plate reinforced by FG-CNTs. Steel Compos Struct 34:289
53. Motezaker M, Eyvazian A (2020) Buckling load optimization of beam reinforced by nanoparticles. Struct Eng Mech 73:481–486
54. Derazkola HA, Eyvazian A, Simchi A (2020) Modeling and experimental validation of material flow during FSW of polycarbonate. Mater Today Commun 22:100796
55. Eyvazian A, Hamouda A, Tarlochan F, Derazkola HA, Khodabakhshi F (2020) Simulation and experimental study of underwater dissimilar friction-stir welding between aluminium and steel. J Mater Res Technol
56. Eyvazian A, Habibi MK, Hamouda AM, Hedayati R (2014) Axial crushing behavior and energy absorption efficiency of corrugated tubes. Mater Des 1980–2015(54):1028–1038
57. Bakhtiari M, Tarkashvand A, Daneshjou K (2020) Plane-strain wave propagation of an impulse-excited fluid-filled functionally graded cylinder containing an internally clamped shell. Thin-Walled Struct 106482
58. Ebrahimi F, Mohammadi K, Barouti MM, Habibi M (2019) Wave propagation analysis of a spinning porous graphene nanoplatelet-reinforced nanoshell. Waves Random Complex Media 1–27
59. Ebrahimi F, Seyfi A (2019) Wave propagation response of multi-scale hybrid nanocomposite shell by considering aggregation effect of CNTs. Mech Based Des Struct Mach 1–22
60. Karami B, Shahsavari D, Janghorban M, Dimitri R, Tornabene F (2019) Wave propagation of porous nanoshells. Nanomaterials 9:22
61. Ebrahimi F, Barati MR (2016) Magneto-electro-elastic buckling analysis of nonlocal curved nanobeams. Eur Phys J Plus 131:346
62. Ebrahimi F, Barati MR (2018) Vibration analysis of piezoelectrically actuated curved nanosize FG beams via a nonlocal strain-electric field gradient theory. Mech Adv Mater Struct 25:350–359
63. Ebrahimi F, Barati MR (2016) On nonlocal characteristics of curved inhomogeneous Euler-Bernoulli nanobeams under different temperature distributions. Appl Phys A 122:880
64. Ebrahimi F, Barati MR (2017) Size-dependent dynamic modeling of inhomogeneous curved nanobeams embedded in elastic medium based on nonlocal strain gradient theory. Proc Inst Mech Eng Part C J Mech Eng Sci 231:4457–4469
65. Ebrahimi F, Barati MR, Mahesh V (2019) Dynamic modeling of smart magneto-electro-elastic curved nanobeams. Adv Nano Res 7:145
66. Mirjavadi SS, Forsat M, Barati MR, Hamouda A (2020) Post-buckling of higher-order stiffened metal foam curved shells with porosity distributions and geometrical imperfection. Steel Compos Struct 35:567–578
67. Mirjavadi SS, Forsat M, Barati MR, Hamouda AS (2020) Geometrically nonlinear vibration analysis of eccentrically stiffened porous functionally graded annular spherical shell segments. Mech Based Des Struct Mach 1–15
68. Qu S, Zhao L, Xiong Z (2020) Cross-layer congestion control of wireless sensor networks based on fuzzy sliding mode control. Neural Comput Appl 1–16
69. Zhang H, Qu S, Li H, Luo J, Xu W (2020) A moving shadow elimination method based on fusion of multi-feature. IEEE Access 8:63971–63982

70. Pang R, Xu B, Kong X, Zou D (2018) Seismic fragility for high CFRDs based on deformation and damage index through incremental dynamic analysis. Soil Dyn Earthq Eng 104:432–436
71. Pang R, Xu B, Zhou Y, Zhang X, Wang X (2020) Fragility analysis of high CFRDs subjected to mainshock-aftershock sequences based on plastic failure. Eng Struct 206:110152
72. Guo J, Zhang X, Gu F, Zhang H, Fan Y (2020) Does air pollution stimulate electric vehicle sales? Empirical evidence from twenty major cities in China. J Clean Product 249:119372
73. Zeng H-B, Teo KL, He Y, Wang W (2019) Sampled-data-based dissipative control of TS fuzzy systems. Appl Math Model 65:415–427
74. Gao N-S, Guo X-Y, Cheng B-Z, Zhang Y-N, Wei Z-Y, Hou H (2019) Elastic wave modulation in hollow metamaterial beam with acoustic black hole. IEEE Access 7:124141–124146
75. Chen H, Zhang G, Fan D, Fang L, Huang L (2020) Nonlinear lamb wave analysis for microdefect identification in mechanical structural health assessment. Measurement 108026
76. Gao N, Wei Z, Hou H, Krushynska AO (2019) Design and experimental investigation of V-folded beams with acoustic black hole indentations. J Acoust Soc Am 145:EL79–EL83
77. Song Q, Zhao H, Jia J, Yang L, Lv W, Gu Q et al (2020) Effects of demineralization on the surface morphology, microcrystalline and thermal transformation characteristics of coal. J Anal Appl Pyrol 145:104716
78. Moayedi H, Hayati S (2018) Applicability of a CPT-based neural network solution in predicting load-settlement responses of bored pile. Int J Geomech 18
79. Moayedi H, Bui DT, Foong LK (2019) Slope stability monitoring using novel remote sensing based fuzzy logic. Sensors (Switzerland) 19
80. Moayedi H, Bui DT, Kalantar B, Osouli A, Gör M, Pradhan B et al (2019) Harris hawks optimization: a novel swarm intelligence technique for spatial assessment of landslide susceptibility. Sensors (Switzerland) 19
81. Moayedi H, Mu'azu MA, Kok Foong L (2019) Swarm-based analysis through social behavior of grey wolf optimization and genetic programming to predict friction capacity of driven piles. Eng Comput
82. Moayedi H, Osouli A, Nguyen H, Rashid ASA (2019) A novel Harris hawks' optimization and k-fold cross-validation predicting slope stability. Eng Comput
83. Yuan C, Moayedi H (2019) The performance of six neural-evolutionary classification techniques combined with multi-layer perception in two-layered cohesive slope stability analysis and failure recognition. Eng Comput
84. Yuan C, Moayedi H (2019) Evaluation and comparison of the advanced metaheuristic and conventional machine learning methods for the prediction of landslide occurrence. Eng Comput
85. Zhao X, Li D, Yang B, Ma C, Zhu Y, Chen H (2014) Feature selection based on improved ant colony optimization for online detection of foreign fiber in cotton. Appl Soft Comput 24:585–596
86. Wang M, Chen H (2020) Chaotic multi-swarm whale optimizer boosted support vector machine for medical diagnosis. Appl Soft Comput 88:105946
87. Zhao X, Zhang X, Cai Z, Tian X, Wang X, Huang Y et al (2019) Chaos enhanced grey wolf optimization wrapped ELM for diagnosis of paraquat-poisoned patients. Comput Biol Chem 78:481–490
88. Xu X, Chen H-L (2014) Adaptive computational chemotaxis based on field in bacterial foraging optimization. Soft Comput 18:797–807
89. Shen L, Chen H, Yu Z, Kang W, Zhang B, Li H et al (2016) Evolving support vector machines using fruit fly optimization for medical data classification. Knowl-Based Syst 96:61–75
90. Wang M, Chen H, Yang B, Zhao X, Hu L, Cai Z et al (2017) Toward an optimal kernel extreme learning machine using a chaotic moth-flame optimization strategy with applications in medical diagnoses. Neurocomputing 267:69–84
91. Xu Y, Chen H, Luo J, Zhang Q, Jiao S, Zhang X (2019) Enhanced Moth-flame optimizer with mutation strategy for global optimization. Inf Sci 492:181–203
92. Chen H, Zhang Q, Luo J, Xu Y, Zhang X (2020) An enhanced Bacterial Foraging Optimization and its application for training kernel extreme learning machine. Appl Soft Comput 86:105884
93. Li C, Han Q, Wang Z, Wu X (2020) Analysis of wave propagation in functionally graded piezoelectric composite plates reinforced with graphene platelets. Appl Math Model
94. Ebrahimi F, Dabbagh A (2018) Thermo-magnetic field effects on the wave propagation behavior of smart magnetostrictive sandwich nanoplates. Eur Phys J Plus 133:97
95. Abad F, Rouzegar J (2019) Exact wave propagation analysis of moderately thick Levy-type plate with piezoelectric layers using spectral element method. Thin-Walled Struct 141:319–331
96. Habibi M, Mohammadgholiha M, Safarpour H (2019) Wave propagation characteristics of the electrically GNP-reinforced nanocomposite cylindrical shell. J Braz Soc Mech Sci Eng 41:221
97. Tornabene F, Bacciocchi M, Fantuzzi N, Reddy J (2019) Multiscale approach for three-phase CNT/polymer/fiber laminated nanocomposite structures. Polym Compos 40:E102–E126
98. Karimiasl M, Ebrahimi F, Vinyas M (2019) Nonlinear vibration analysis of multiscale doubly curved piezoelectric composite shell in hygrothermal environment. J Intell Mater Syst Struct 30:1594–1609
99. Shariati A, Mohammad-Sedighi H, Żur KK, Habibi M, Safa M (2020) On the vibrations and stability of moving viscoelastic axially functionally graded nanobeams. Materials 13:1707
100. Batou B, Nebab M, Bennai R, Atmane HA, Tounsi A, Bouremana M (2019) Wave dispersion properties in imperfect sigmoid plates using various HSDTs. Steel Compos Struct 33:699
101. Pham Q-H, Pham T-D, Trinh QV, Phan D-H (2019) Geometrically nonlinear analysis of functionally graded shells using an edge-based smoothed MITC3 (ES-MITC3) finite elements. Eng Comput 1–14
102. Salah F, Boucham B, Bourada F, Benzair A, Bousahla AA, Tounsi A (2019) Investigation of thermal buckling properties of ceramic-metal FGM sandwich plates using 2D integral plate model. Steel Compos Struct 33:805
103. Ebrahimi F, Nouraei M, Dabbagh A (2019) Thermal vibration analysis of embedded graphene oxide powder-reinforced nanocomposite plates. Eng Comput 1–17
104. Moayedi H, Darabi R, Ghabussi A, Habibi M, Foong LK (2020) Weld orientation effects on the formability of tailor welded thin steel sheets. Thin-Walled Struct 149:106669
105. Shariati A, Habibi M, Tounsi A, Safarpour H, Safa M Application of exact continuum size-dependent theory for stability and frequency analysis of a curved cantilevered microtubule by considering viscoelastic properties
106. Moayedi H, Habibi M, Safarpour H, Safarpour M, Foong L Buckling and frequency responses of a graphen nanoplatelet reinforced composite microdisk. Int J Appl Mech
107. Moayedi H, Aliakbarlou H, Jebeli M, Noormohammadiarani O, Habibi M, Safarpour H et al (2020) Thermal buckling responses of a graphene reinforced composite micropanel structure. Int J Appl Mech 12:2050010
108. Ghabussi A, Ashrafi N, Shavalipour A, Hosseinpour A, Habibi M, Moayedi H et al (2019) Free vibration analysis of an electro-elastic GPLRC cylindrical shell surrounded by viscoelastic foundation using modified length-couple stress parameter. Mech Based Des Struct Mach 1–25

109. Habibi M, Mohammadi A, Safarpour H, Shavalipour A, Ghadiri M (2019) Wave propagation analysis of the laminated cylindrical nanoshell coupled with a piezoelectric actuator. Mech Based Des Struct Mach 1–19
110. Ghazanfari A, Soleimani SS, Keshavarzzadeh M, Habibi M, Assempuor A, Hashemi R (2019) Prediction of FLD for sheet metal by considering through-thickness shear stresses. Mech Based Des Struct Mach 1–18
111. Mohammadi A, Lashini H, Habibi M, Safarpour H (2019) Influence of viscoelastic foundation on dynamic behaviour of the double walled cylindrical inhomogeneous micro shell using MCST and with the aid of GDQM. J Solid Mech 11:440–453
112. Habibi M, Payganeh G (2018) Experimental and finite element investigation of titanium tubes hot gas forming and production of square cross-section specimens
113. Fazaeli A, Habibi M, Ekrami A (2016) Experimental and finite element comparison of mechanical properties and formability of dual phase steel and ferrite-pearlite steel with the same chemical composition. Metall Eng 19(2):84–93
114. Shokrgozar A, Ghabussi A, Ebrahimi F, Habibi M, Safarpour H (2020) Viscoelastic dynamics and static responses of a graphene nanoplatelets-reinforced composite cylindrical microshell. Mech Based Des Struct Mach 1–28
115. Adamian A, Safari KH, Sheikholeslami M, Habibi M, Al-Furjan M, Chen G (2020) Critical temperature and frequency characteristics of GPLs-reinforced composite doubly curved panel. Appl Sci 10:3251
116. Ghadiri M, Shafiei N, Safarpour H (2017) Influence of surface effects on vibration behavior of a rotary functionally graded nanobeam based on Eringen's nonlocal elasticity. Microsyst Technol 23:1045–1065
117. Habibi M, Hashemi R, Tafti MF, Assempour A (2018) Experimental investigation of mechanical properties, formability and forming limit diagrams for tailor-welded blanks produced by friction stir welding. J Manuf Process 31:310–323
118. Habibi M, Hashemi R, Sadeghi E, Fazaeli A, Ghazanfari A, Lashini H (2016) Enhancing the mechanical properties and formability of low carbon steel with dual-phase microstructures. J Mater Eng Perform 25:382–389
119. Reddy JN (2003) Mechanics of laminated composite plates and shells: theory and analysis. CRC Press, London
120. Shamsaddini Lori E, Ebrahimi F, Elianddy Bin Supeni E, Habibi M, Safarpour H (2020) The critical voltage of a GPL-reinforced composite microdisk covered with piezoelectric layer. Eng Comput
121. Moayedi H, Ebrahimi F, Habibi M, Safarpour H, Foong LK (2020) Application of nonlocal strain–stress gradient theory and GDQEM for thermo-vibration responses of a laminated composite nanoshell. Eng Comput
122. Safarpour M, Ebrahimi F, Habibi M, Safarpour H (2020) On the nonlinear dynamics of a multi-scale hybrid nanocomposite disk. Eng Comput 1–20
123. Ebrahimi F, Supeni EEB, Habibi M, Safarpour H (2020) Frequency characteristics of a GPL-reinforced composite microdisk coupled with a piezoelectric layer. Eur Phys J Plus 135:144
124. Ghayesh MH (2019) Viscoelastic mechanics of Timoshenko functionally graded imperfect microbeams. Compos Struct 225:110974
125. Ghayesh MH (2012) Subharmonic dynamics of an axially accelerating beam. Arch Appl Mech 82:1169–1181
126. Kazemirad S, Ghayesh MH, Amabili M (2013) Thermo-mechanical nonlinear dynamics of a buckled axially moving beam. Arch Appl Mech 83:25–42
127. Shariati A, Ghabussi A, Habibi M, Safarpour H, Safarpour M, Tounsi A et al (2020) Extremely large oscillation and nonlinear frequency of a multi-scale hybrid disk resting on nonlinear elastic foundation. Thin-Walled Struct 154:106840
128. Al-Furjan M, Habibi M, Safarpour H (2020) Vibration control of a smart shell reinforced by graphene nanoplatelets. Int J Appl Mech
129. Habibi M, Safarpour M, Safarpour H (2020) Vibrational characteristics of a FG-GPLRC viscoelastic thick annular plate using fourth-order Runge-Kutta and GDQ methods. Mech Based Des Struct Mach 1–22
130. Liu Z, Su S, Xi D, Habibi M (2020) Vibrational responses of a MHC viscoelastic thick annular plate in thermal environment using GDQ method. Mech Based Des Struct Mach 1–26
131. Al-Furjan M, Safarpour H, Habibi M, Safarpour M, Tounsi A (2020) A comprehensive computational approach for nonlinear thermal instability of the electrically FG-GPLRC disk based on GDQ method. Eng Comput 1–18
132. Jermsittiparsert K, Ghabussi A, Forooghi A, Shavalipour A, Habibi M, won Jung D et al (2020) Critical voltage, thermal buckling and frequency characteristics of a thermally affected GPL reinforced composite microdisk covered with piezoelectric actuator. Mech Based Des Struct Mach 1–23
133. Ghayesh MH (2019) Resonant vibrations of FG viscoelastic imperfect Timoshenko beams. J Vib Control 25:1823–1832
134. Ghayesh MH, Amabili M (2013) Nonlinear vibrations and stability of an axially moving Timoshenko beam with an intermediate spring support. Mech Mach Theory 67:1–16
135. Ghayesh MH, Amabili M (2013) Nonlinear dynamics of an axially moving Timoshenko beam with an internal resonance. Nonlinear Dyn 73:39–52
136. Ghayesh MH (2012) Nonlinear dynamic response of a simply-supported Kelvin-Voigt viscoelastic beam, additionally supported by a nonlinear spring. Nonlinear Anal Real World Appl 13:1319–1333
137. Ghayesh MH (2019) Mechanics of viscoelastic functionally graded microcantilevers. Eur J Mech-A/Solids 73:492–499
138. Ebrahimi F, Dabbagh A (2019) Vibration analysis of multi-scale hybrid nanocomposite plates based on a Halpin-Tsai homogenization model. Compos B Eng 173:106955
139. Wattanasakulpong N, Chaikittiratana A (2015) Exact solutions for static and dynamic analyses of carbon nanotube-reinforced composite plates with Pasternak elastic foundation. Appl Math Model 39:5459–5472
140. Khdeir A (1988) Free vibration and buckling of symmetric cross-ply laminated plates by an exact method. J Sound Vib 126:447–461
141. Thinh TI, Nguyen MC, Ninh DG (2014) Dynamic stiffness formulation for vibration analysis of thick composite plates resting on non-homogenous foundations. Compos Struct 108:684–695